UC Berkeley
UC Berkeley Previously Published Works

Title

1-D modeling of radionuclide transport via heterogeneous geological formations for arbitrary length decay chains using numerical inversion of Laplace transforms

Permalink

Authors

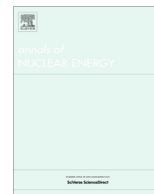van den Akker, Bret Patrick
Ahn, Joonhong

Publication Date

DOI

Copyright Information

Peer reviewed

CrossMark

1-D modeling of radionuclide transport via heterogeneous geological formations for arbitrary length decay chains using numerical inversion of Laplace transforms

Bret Patrick van den Akker, Joonhong Ahn *

Department of Nuclear Engineering, University of California at Berkeley, Berkeley, CA 94720-1730, United States

ABSTRACT

We present the Laplace-transformed analytical solution (LTAS) to the one-dimensional radionuclide transport equation for an arbitrary length decay-chain through an arbitrary combination of multiply fractured and porous transport segments subject to an arbitrary time-dependent release mode at the entrance point to the series of transport segments. The LTAS may be numerically inverted to obtain the time-dependent concentration of the radionuclides of interest at an arbitrary down gradient location. For a special case, where the source function is defined as the band release with a single radionuclide without precursors, the Laplace inverse transformation could be performed analytically, yielding a closed-form analytical solution. A computer code, TTBX, has been developed by implementing the LTAS, and benchmarked against the closed-form analytical solution. Numerical examples are presented to demonstrate the utility of these solutions and the importance of increased fidelity in the transport pathway for reliable performance assessment for the geological disposal of spent nuclear fuels.

© 2013 Elsevier Ltd. All rights reserved.

1. Introduction

The transport of radionuclides via fractured and porous media is one of the main pathways included in exposure scenarios for the intake of radioactive materials released from nuclear waste disposed in geological repositories. Additionally, the study of the transport of radionuclides has important implications in the investigation of the normal and accidental releases of radionuclides from nuclear facilities.

Studies of the transport of radionuclides in discrete fractures considering the effects of matrix diffusion were begun in the 1980s (Neretnieks, 1980). Subsequent studies used mathematical models and parametric sensitivity analysis to ascertain the effects of longitudinal hydrodynamic dispersion on the transport of contaminants (Rasmuson and Nereetnieks, 1981; Tang et al., 1981). Attempts to obtain analytical solutions which include the effects of multi-member decay chains for specialized cases were also made (Sudicky and Frind, 1984; Chambré et al., 1982). A 1-D model for the transport of radionuclides through a single type of permeable or fractured rock using the numerical inversion of Laplace transforms was developed in Hodgkinson and Maul (1988) and implemented in Ahn (1998) by the addition of a solubility-limited source term model. In addition to these analytical studies, several

numerical schemes have been developed which implement the finite element method or the integrated finite difference method (Ahn et al., 1984; Grisak and Pickens, 1980; Rasmuson et al., 1982).

In this study, a model for the release and transport of radionuclides through heterogeneous geological media is presented. The model accommodates a heterogeneous transport pathway through an arbitrary number of rock types and admits a decay chain which consists of an arbitrary number of members, subject to an arbitrary time-dependent radionuclide release mode at the entrance point into a series of transport segments. The model considers the effects of advection, sorption retardation in the transport pathway, matrix diffusion, and radioactive decay and in-growth.

The Laplace-transformed analytical solutions (LTAS) are presented and numerical results are obtained by numerical inversion of the LTAS using Talbot's method (Talbot, 1978). A computer code TTBX has been developed by utilizing LTAS and the Talbot's method, based on the readily available code TTB for the single-region model (Ahn, 1998).

For the simplified situation, where a single radionuclide without precursors is considered to be released into the heterogeneous transport pathway with the band-release mode (van den Akker, 2012), Laplace inverse transform could be analytically performed, yielding a closed-form analytical solution. This analytical solution has been used for the benchmarking of the TTBX code, as well as for evaluation of fission-product radionuclides, such as ^{99}Tc and ^{129}I, which are known to be the major contributors to the radiolog-

---

Nomenclature

A_p	the area of the pth transport segment opening (m^2)
b_p	fracture half-aperture of pth fracture segment (m)
$BDCF_j$	biosphere dose conversion factor (BDCF) for radionuclide j (Sv/yr/(Bq/m^3))
$C_j(x\,t)$	time-dependent concentration of radionuclide j in the groundwater at the observation location x (Bq/m^3).
$D_T(x,t)$	total time-dependent dose to the RMEI from the N transported radionuclides to the observation location x at time t (Sv/yr).
t	time after the beginning of the release of nuclides (s) at the source
w_p	characteristic width of fracture opening (m) of segment p
x	total distance to the observation location along the transport pathway (m)
x_p	transport distance of the pth transport segment (m)
v_p	water velocity in the pth transport segment (m s^{-1})
z_p	distance from the fracture surface into the host rock media in the pth transport segment (m)
ε_p	porosity of rock matrix associated with the pth segment
ϕ_p	Porosity of the material filling the pth transport segment
ρ_p	density of material filling the pth transport segment (kg m^{-3})
ρ'_p	density of rock matrix associated with the pth segment (kg m^{-3})
$B_p(x,t)$	function defined in (40)
$ERFC(\cdot)$	complementary error function
$h(\cdot)$	Heaviside function
N_0	initial release rate of the radionuclide at $x = 0$, $t = 0$ (mol s^{-1}) for the band release
t_R	retarded transport time along pathway (s)

T	duration of band release (s)
a_p	length of diffusion path in rock matrix associated with the pth segment (m)
$B_{p_{qn}}(s)$	functions defined in (28) (s^{-1})
$C_{p_n}(x,t)$	concentration of the nth nuclide in the water phase in the pth transport segment (mol m^{-3})
$\widehat{C_{p_n}}(x,t)$	Laplace transform of $C_n^p(x,t)$ (mol s m^{-3})
D_{p_n}	matrix diffusion coefficient for the nth nuclide in the pth fracture segments (m^2 s^{-1})
$F_n(t)$	source term for the nth nuclide (mol s^{-1})
$\widehat{F}_n(s)$	Laplace transform of $F_n(t)$ (mol)
$g_{p_m}(s)$	functions defined in (34) and (32) (s^{-1})
K_{p_n}	equilibrium sorption coefficient for the nth nuclide on the material filling the pth transport segment (m^3 kg^{-1})
K'_{p_m}	equilibrium sorption coefficient for the nth nuclide in rock matrix associated with the pth segment (m^3 kg^{-1})
R_{p_n}	retardation coefficient for nth nuclide for the material filling the pth transport segment
$S_{p_i}(s)$	functions defined in (19) and (20) (mol s m^{-3})
$u_{p_{mn}}(s)$	functions defined in (26) and (33)
$W_{p_n}(x,z_p,t)$	concentration of the nth nuclide in the pores of the rock matrix associated with the pth fracture segment (mol m^{-3})
$\widehat{W_{p_n}}(x,z_p,t)$	Laplace transform of $W_{p_n}(x,z_p,t)$ (mol s m^{-3})
$Y_{p_{mn}}(z_p,s)$	functions defined in (22) and (23)
α_{p_n}	capacity factor for the nth nuclide in the rock matrix associated with the pth segment
$\theta_{p_m}(s)$	functions defined in (25) (m^{-1})
λ_n	decay constant for the nth nuclide (s^{-1})
$\xi_{p_{im}}(s)$	functions defined in (30) and (35)
$\sigma_{p_m}(s)$	functions defined in (18) (mol m^{-3})

ical impact of a deep geological repository for high-level wastes and spent nuclear fuels.

Numerical illustration of the new code TTBX is given for the case reported previously for disposal of TRISO spent fuel at the Yucca Mountain Repository (van den Akker and Ahn, 2013), to observe effects of considering heterogeneity along the transport pathway on results of total performance assessment of a geological repository.

## 2. Physical processes, assumptions, and conceptual model

The transport pathway between the source and the end point (x) is assumed to occur along an arbitrary number of interconnected 1-D segments of water-saturated rocks (Fig. 1). The end point is usually set at the point, where radionuclides enter the biosphere, such as a well for drinking and irrigation.

Each segment includes the water-conductive part, through which radionuclides are transported by advection. In segment p, the water flows at a constant mean pore velocity in the segment of v_p through either the permeable porous rock or the fracture filled with the material with porosity ϕ_p. If the segment is characterized as porous rock, the cross-sectional area of the conductive part of the segment is denoted as A_p. If the conductive part of the segment is characterized as a fracture, the fracture aperture is denoted as $2b_p$. Note that the effects of hydrodynamic dispersion along the water-conductive part are not explicitly included in the present conceptual model. These effects may be modeled by a statistical sampling of the groundwater velocity over an appropriate

probability distribution function (Arriaza and Ghezzehei, 2013; Singhal and Gupta, 2010); therefore their exclusion from the governing equations does not affect the generality of this model. The assumptions of no hydrodynamic dispersion and complete mixing across the cross sectional area of the conduit allows one-dimensional "plug flow" transport of radionuclides in the segment.

At the interface between two consecutive segments, say p and $p + 1$, the in-coming plug flow from the p side with homogeneous contamination across the cross section is instantaneously re-distributed homogeneously over the cross section of the $p + 1$ side. Thus, the mass of a radionuclide is conserved at the interface point. In this model, we do not strictly enforce mass conservation of the water between segments; thus the pore velocity v_p is set a priori. This could be interpreted, for instance, as the dilution of the nuclide concentration as the result of the infiltration of fresh groundwater at the boundary interface. A great deal of latitude is given to the user to determine the cross-sectional area A_p of the transport segments. In the case of a fractured segment the cross-sectional area will be determined as the product of the fracture aperture $2b_p$ and the characteristic width of that fracture segment w_p. A reasonable consideration for many heterogeneous transport pathways may be to consider that the volumetric flow of water through each of the pth segments will be conserved, so that the cross-sectional area of each of the transport segments following the first will be scaled to preserve this quantity.

In the case of a fracture segment, molecular diffusion with the matrix diffusion coefficient D_{p_n} perpendicular to the fracture face into rock matrix filled with stationary water is considered. In the case of a porous-rock segment, molecular diffusion perpendicular
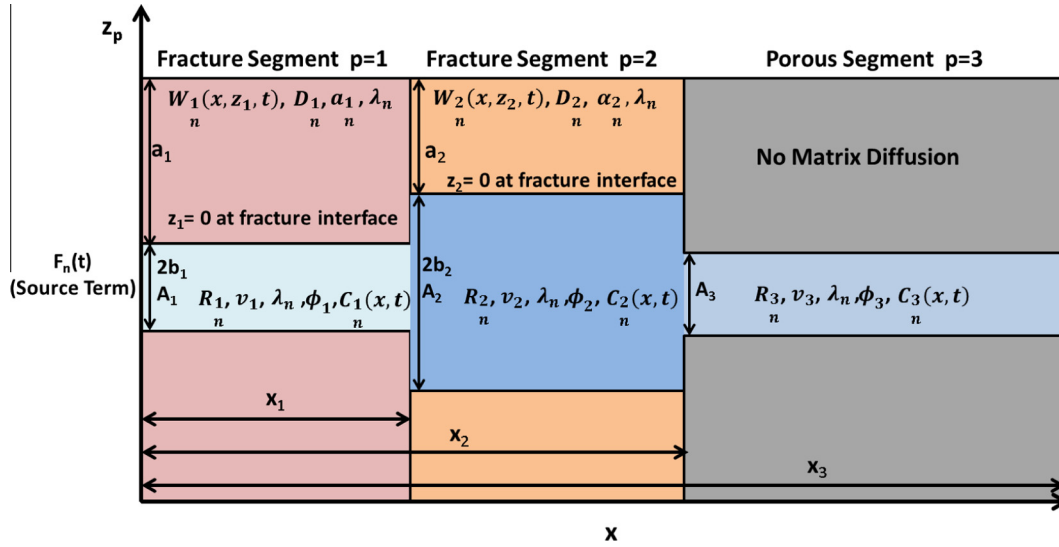
Fig. 1. An example of a potential transport path through heterogeneous geological formations showing the major quantities of interest and physical processes considered. Here two fracture segments join with a porous segment to form the transport path.

to the principal advection direction is not considered. The effects of radioactive decay and ingrowth are incorporated with the parameter λ_n. Sorption equilibrium is accounted for with the material in the conductive part of a segment leading to a retardation factor in each transport segment of R_{p_n} for each member of the decay chain. Sorption equilibrium is also considered for the matrix diffusion in the case of a fracture segment by the capacity factor of the rock matrix α_{p_n} of the rock matrix. It should be noted that the analysis of flow and transport in fractured rocks using matrix diffusion effects is valid for a situation where fracture spacing is sufficiently dense, so that the fractured media acts in a hydraulically similar manner to granular porous media. This approach is applicable for the macroscopic regime where properties are only a function of position and do not vary with the size of the field.

Radionuclide release to the first segment is represented by a general time-dependent function, $F_n(t)$, for nuclide n. This can be determined by considering the physical processes in the near-field region that contains a waste package and engineered barriers surrounding the package. In the previous study (Ahn, 1998), where the computer code TTB was developed, a model was developed to formulate $F_n(t)$ by considering solubility-limited release of hardly-soluble species by waste-form dissolution and subsequent diffusional transport with multi-member decay chains. In the present study, we have adopted the same model as (Ahn, 1998), and develop a computer code TTBX, as we discuss further in Section 4.

3. Mathematical formulation

We consider here the governing equations primarily for a fracture segment. The governing equation for a porous segment may be recovered from the equations for the fracture segment by setting the matrix diffusion coefficient (D_p) equal to zero and neglecting the governing equation for the concentration of the radionuclide in the host rock matrix.

3.1. Governing equations and side conditions

The governing equations with $\lambda_0 = 0$ and $x_0 = 0$ are written by referring to the work by Hodgkinson and Maul (1988). In the present formulation, index p is added to denote individual segments along the pathway. The range of variable x is defined in each segment accordingly.

$$R_{p_n}\frac{\partial C_{p_n}(x,t)}{\partial t} + v_p\frac{\partial C_{p_n}(x,t)}{\partial x} - \frac{D_{p_n}}{b_p}\frac{\partial W_{p_n}(x,z_p,t)}{\partial z_p}\bigg|_{z_p=0}$$
$$= \lambda_{n-1}R_{p_{n-1}}C_{p_{n-1}}(x,t) - \lambda_n R_{p_n}C_{p_n}(x,t),$$
$$x_p \geqslant x \geqslant x_{p-1}, \ t>0, \ p=1,2,3,\ldots, \quad (1)$$

and

$$\alpha_{p_n}\frac{\partial W_{p_n}(x,z_p,t)}{\partial t} - D_{p_n}\frac{\partial^2 W_{p_n}(x,z_p,t)}{\partial z_p^2}$$
$$= \lambda_{n-1}\alpha_{p_{n-1}}W_{p_{n-1}}(x,z_p,t) - \lambda_n \alpha_{p_n}W_{p_n}(x,z_p,t)$$
$$z_p > 0, \quad x_p \geqslant x \geqslant x_{p-1}, \ t>0, \ p=1,2,3,\ldots, \quad (2)$$

where

$$R_{p_n} = 1 + \frac{\rho_p(1-\phi_p)}{\phi_p}K_{p_n}, \quad p=1,2,3,\ldots,\text{and} \quad (3)$$

$$\alpha_{p_n} = \epsilon_p + \rho'_p K'_{p_n}, \quad p=1,2,3\ldots \quad (4)$$

Here, R_{p_n} and α_{p_n} are the retardation factor of the nth radionuclide for the material filling the pth transport segment and the capacity factor of the nth radionuclide in for the matrix diffusion in the case the pth segment is characterized as a fracture segment, respectively.

The governing equations are subject to the following initial and boundary conditions:

$$C_{p_n}(x,0) = 0, \quad x_p \geqslant x \geqslant x_{p-1}, \ p=1,2,3,\ldots, \quad (5)$$

$$C_{1_n}(0,t) = \frac{F_n(t)}{v_1\phi_1 A_1}, \quad t>0, \quad (6)$$

$$v_p\phi_p A_p C_p(x_p,t) = v_{p+1}\phi_{p+1}A_{p+1}C_p(x_p,t), \quad t>0, \ p=1,2,3,\ldots, \quad (7)$$

$$W_{p_n}(x,z_p,0) = 0, \quad z_p>0, x_0=0, \ x_p \geqslant x \geqslant x_{p-1}, \ p=1,2,3\ldots \quad (8)$$

$$W_{p_n}(x,0,t) = C_{p_n}(x,t), \quad t>0, \ x_p \geqslant x \geqslant x_{p-1}, \ p=1,2,3,\ldots, \quad (9)$$

$$\frac{\partial W_{p_n}(x,z_p,t)}{\partial z_p}\bigg|_{z_p=a_p} = 0, \quad z_p>0, \ t>0, \ x>0, \ p=1,2,3,\ldots, \quad (10)$$

where $C_{p_n}(x,t)$ is the concentration of the nth member of the decay chain in the pth transport segment; $W_{p_n}(x,z_p,t)$, the concentration of the nth member of the decay chain in the pores of the rock matrix associated with the pth transport segment; $F_n(t)$ is the source term for the nth radionuclide at the transport pathway genesis. Variables with one subscript are independent of either the transport segment number or the position in the decay chain (e.g. λ_n and v_p, respectively). Eq. (7) indicates the mass conservation of radionuclide n at the interface between two consecutive segments p and $p + 1$.

The Laplace-transformed governing equations are given as:

$$R_{p_n}(s+\lambda_n)\widehat{C_{p_n}}(x,s) + v_p\frac{d\widehat{C_{p_n}}(x,s)}{dx} - \frac{D_{p_n}}{b_p}\frac{d\widehat{W_{p_n}}(x,z_p,s)}{dz_p}\bigg|_{z_p=0}$$
$$= \lambda_{n-1}R_{p_{n-1}}\widehat{C_{p_{n-1}}}(x,s), \quad x_p \geqslant x \geqslant x_{p-1}, \ p=1,2,3,\ldots, \quad (11)$$

$$\alpha_{p_n}(s+\lambda_n)\widehat{W_{p_n}}(x,z_p,s) - D_{p_n}\frac{d^2\widehat{W_{p_n}}(x,z_p,s)}{dz_p^2}$$
$$= \lambda_{n-1}\alpha_{p_{n-1}}\widehat{W_{p_{n-1}}}(x,z_p,s) \ z_p > 0, \ x_p \geqslant x \geqslant x_{p-1}, \ p=1,2,3,\ldots, \quad (12)$$

subject to the boundary conditions:

$$\widehat{C_{1_n}}(0,s) = \frac{\widehat{F_n}(s)}{v_1\phi_1 A_1} \quad (13)$$

$$v_p\phi_p A_p\widehat{C_{p_n}}(x_p,s) = v_{p+1}\phi_{p+1}A_{p+1}\widehat{C_{p+1_n}}(x_p,s), \quad p=1,2,3,\ldots, \quad (14)$$

$$\widehat{W_{p_n}}(x,0,s) = \widehat{C_{p_n}}(x,s) \quad ,x_0=0, \ x_p \geqslant x \geqslant x_{p-1}, \ p=1,2,3,\ldots, \quad (15)$$

and

$$\frac{d\widehat{W_{p_n}}(x,z_p,s)}{dz_p}\bigg|_{z_p=a_p} = 0, \quad z_p > 0, \ x_p \geqslant x \geqslant x_{p-1}, \ p=1,2,3,\ldots. \quad (16)$$

Here the symbol $\widehat{\ }$ represents the Laplace-transformed quantity and s the Laplace variable.

3.2. Laplace transformed solutions

The recursive solution for the Laplace-transformed concentration along the transport pathway is given as follows:

$$\widehat{C_{p_n}}(x,s) = \sum_{m=1}^{n}u_{p_{mn}}(s)\sigma_{p_m}(s)\exp\left(-g_{p_m}(s)\frac{(x-x_{p-1})}{v_p}\right),$$
$$x_p > x > x_{p-1}, \ p=1,2,3,\ldots, \quad (17)$$

$$\sigma_{p_m}(s) = \sum_{i=1}^{m}\xi_{p_{im}}(s)S_{p_i}(s), \quad p=1,2,3,\ldots, \quad (18)$$

$$S_{p_i}(s) = \frac{v_{p-1}\phi_{p-1}A_{p-1}}{v_p\phi_p A_p}\widehat{C_{p-1_i}}(x_{p-1},s), \quad p=1,2,3,\ldots, \quad (19)$$

$$S_{1_i}(s) = \frac{\widehat{F_i}(s)}{v_1\phi_1 A_1} \quad (20)$$

where in the instances of a fractured segment, the concentration of the radionuclide in the pores of the host rock is given by:

$$\widehat{W_{p_n}}(x,z_p,s) = \sum_{m=1}^{n}Y_{p_{mn}}(z_p,s)\widehat{C_{p_n}}(x,s), \ x_{p-1} > x > x_p, \ p=1,2,3,\ldots, \quad (21)$$

$$Y_{p_{mn}}(z_p,s) = \left(\prod_{k=m}^{n-1}\frac{\alpha_{p_k}\lambda_k}{D_{p_{k+1}}}\right)\sum_{k=m}^{n}\frac{Y_{p_{kk}}(z_p,s)}{\prod_{l=m,l\neq k}^{n}\left[\theta_{p_l}^2(s)-\theta_{p_k}^2(s)\right]}, \quad p=1,2,3,\ldots, \quad (22)$$

$$Y_{p_{nn}}(z_p,s) = \frac{\cosh(\theta_{p_n}(s)(a_p-z_p))}{\cosh(\theta_{p_n}(s)a_p)}, \quad p=1,2,3,\ldots, \quad (23)$$

and the following definitions and recursive relations hold,

$$g_{p_m}(s) = \left(R_{p_m}(s+\lambda_m) - \frac{D_{p_m}\theta_{p_m}(s)}{b_p}\right), \quad p=1,2,3,\ldots, \quad (24)$$

$$\theta_{p_m}(s) = \sqrt{\frac{(s+\lambda_m)\alpha_{p_m}}{D_{p_m}}}, \quad p=1,2,3,\ldots, \quad (25)$$

$$\left(g_{p_n}(s)-g_{p_m}(s)\right)u_{p_{mn}}(s) = R_{p_{n-1}}\lambda_{n-1}u_{p_{mn-1}}(s) + \sum_{q=m}^{n-1}B_{p_{qn}}(s)u_{p_{mq}}(s),$$
$$p=1,2,3,\ldots, \quad (26)$$

$$u_{p_{nn}}(s) = 1, \quad p=1,2,3,\ldots, \quad (27)$$

$$B_{p_{qn}}(s) = -\frac{D_{p_n}}{b_p}\left(\prod_{l=q}^{n-1}\frac{\alpha_{p_l}\lambda_l}{D_{p_{l+1}}}\right)\sum_{l=q}^{n}\frac{\theta_{p_l}(s)\tanh(\theta_{p_l}(s)a_p)}{\prod_{j=q,j\neq l}^{n}\left[\theta_{p_j}^2(s)-\theta_{p_l}^2(s)\right]}, \quad p=1,2,3,\ldots, \quad (28)$$

$$\sigma_{p_m}(s) = \sum_{i=1}^{m}\xi_{p_{im}}(s)S_{p_i}, \quad p=1,2,3,\ldots, \quad (29)$$

$$\xi_{p_{im}}(s) = -\sum_{j=i}^{m-1}u_{p_{jm}}(s)\xi_{p_{ij}}(s), \quad p=1,2,3,\ldots, \quad (30)$$

$$\xi_{p_{mm}}(s) = 1, \quad p=1,2,3,\ldots, \quad (31)$$

and in the instances of a porous transport segment, the following hold:

$$g_{p_m}(s) = R_{p_m}(s+\lambda_m), \quad p=1,2,3,\ldots, \quad (32)$$

$$u_{p_{mn}}(s) = \prod_{k=m}^{n-1}\frac{R_{p_k}\lambda_k}{\left[g_{p_{k+1}}(s)-g_{p_m}(s)\right]}, \quad p=1,2,3,\ldots, \quad (33)$$

$$u_{p_{nn}}(s) = 1, \quad p=1,2,3,\ldots, \quad (34)$$

$$\xi_{p_{im}}(s) = \prod_{k=i}^{m-1}\frac{R_{p_k}\lambda_k}{\left[g_{p_k}(s)-g_{p_m}(s)\right]}, \quad p=1,2,3,\ldots, \quad (35)$$

$$\xi_{p_{mm}}(s) = 1, \quad p=1,2,3,\ldots, \quad (36)$$

3.3. Analytical solution for the band release of a single member decay chain

For the case of the band release (van den Akker, 2012) of a single member decay chain (i.e., $n = 1$) and with a rock matrix of infinite extent for fractured segments (i.e., $a_p \to \infty$), the Laplace-transformed solution obtained in Section 3.2 can be analytically inverted. The band release of a single member decay chain is given as

$$F_1(t) = N_0 e^{-\lambda t}\{h(t) - h(t-T)\}, \quad t > 0, \quad (37)$$

where T is the time duration of the waste form dissolution, the function h is a Heaviside step function, and N_0 is the fictitious initial

release of the radionuclide, determined by assuming (1) congruency between the waste-form dissolution and the radionuclide dissolution into the water phase and (2) negligible hydrodynamic dispersion at the location of waste form dissolution (see van den Akker, 2012 for more detailed discussion on the band release model).

The boundary condition (16), set for the general problem, reads as:

$$\left.\frac{\partial W_p(x,z_p,t)}{\partial z_p}\right|_{z_p\to\infty} = 0, \quad t > 0, \ x > 0, \tag{38}$$

While this simple case is of use as a benchmark for the multi-member decay-chain case, as will be discussed in Section 5, this is also of practical interest since many of the main contributors to the dose delivered to exposed individuals are fission products, and members of a single member decay chain, (e.g. [99]Tc and [129]I). The analytical solution for the band release of a single member decay chain provides for a reliable and conservative calculation of the concentration of radionuclides to reach an arbitrary down gradient location.

The analytical solution for the concentration $C_p(x,t)$ of the radionuclide in the pth transport segment may be expressed as:

$$C_p(x,t) = \frac{N_0 \exp(-\lambda t)}{v_p \phi_p A_p} B_p(x,t), \quad t \geqslant 0, \ x_p \geqslant x \geqslant x_{p-1}, \ p = 1,2,3,\ldots, \tag{39}$$

where

$$B_p(x,t) = h(t-t_R)\mathrm{ERFC}\left(\frac{\left(\sum_{j=1}^{p-1}\frac{\sqrt{D_j\alpha_j}}{b_j v_j}(x_j - x_{j-1})\right) + \frac{\sqrt{D_p\alpha_p}}{b_p v_p}(x - x_{p-1})}{2(t-t_R)^{\frac{1}{2}}}\right)$$
$$-h(t-t_R-T)\mathrm{ERFC}\left(\frac{\left(\sum_{j=1}^{p-1}\frac{\sqrt{D_j\alpha_j}}{b_j v_j}(x_j - x_{j-1})\right) + \frac{\sqrt{D_p\alpha_p}}{b_p v_p}(x - x_{p-1})}{2(t-t_R-T)^{\frac{1}{2}}}\right),$$
$$p = 1,2,3,\ldots, \tag{40}$$

and

$$t_R = \sum_{j=1}^{p-1}\left(\frac{R_j}{v_j}(x_j - x_{j-1})\right) + \frac{R_p}{v_p}(x - x_{p-1}), \quad p = 1,2,3,\ldots. \tag{41}$$

Note that t_R represents the retarded travel time in from the source to the observations point. If there is no retardation along the transport pathway, t_R is simply the total time for water to flow to the observation point. If the entire pathway is characterized as a porous medium, i.e., no matrix diffusion anywhere along the pathway, the arguments of the complimentary error functions becomes zero, resulting in

$$B_p(x,t) = h(t-t_R) - h(t-t_R-T), \quad p = 1,2,3,\ldots,. \tag{40'}$$

4. Code development

4.1. Features of the TTBX code

The LTAS developed in Section 3.2 has been implemented into a computer code called TTBX, which uses Talbot's Method (Talbot, 1978) to invert the LTAS. TTBX is considered a multi-region extension of the existing computer code TTB (Transfer-To-Biosphere) developed at the University of California at Berkeley(Ahn, 1998). TTB was developed to quantify the amount and types of radionuclides which will reach the biosphere resulting from the release of these materials from HLW in a geological repository and subsequent transport via a 1-D planar fracture.

The source term implemented in both TTB and TTBX considers the solubility-limited release of radionuclides from a given waste form and their diffusive transport within a surrounding diffusion
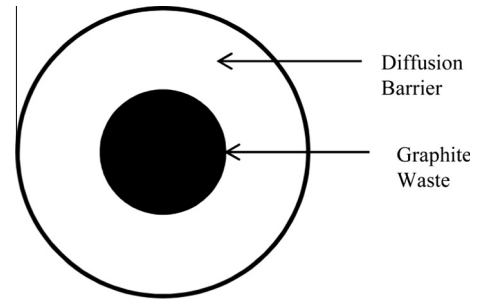

Fig. 2. Geometry in the near field showing spherical waste form and surrounding diffusion barrier.

barrier. Conceptually, a geometric transformation of the radionuclide containing waste form is made into a sphere of waste surrounded by a concentric spherical diffusion barrier region (Fig. 2). Subsequent to contact with groundwater, the waste form begins to dissolve and radionuclides are released. The release of radionuclides is considered to occur by two modes in this source term model; congruent release and solubility limited release. In the case of congruent release, the fractional release rate of the nuclide is equal to the fractional dissolution rate of the waste matrix. If the solubility of an individual radionuclide is low, then a precipitate of the nuclide will form at the waste form surface. The precipitate slowly dissolves at a rate given by the rate of mass transfer into the water in the pores in the surrounding medium, with the concentration of the nuclide in the water adjacent to the surface of the waste form given by its solubility. Note that the radionuclide release mode is determined not only by its solubility, but also by the rate of waste-form dissolution, radionuclide inventory in the waste form, and the rate of diffusive mass transfer at the point of waste-form dissolution. The release mode is determined by considering the material balance of each nuclide. For the transport of the radionuclides through the diffusion barrier we consider the following physical mechanisms: (i) sorption with the diffusion barrier materials, (ii) diffusive transport through the diffusion barrier, and (iii) radioactive decay. The release rate of radionuclides across the outer boundary of the diffusion barrier is determined and is used as the source term for the input for the radionuclides in the far-field transport calculations. The complete mathematical formulation of the source term may be found in Ahn (1998).

4.2. Benchmarking

One of the many benefits of having developed, in Section 3.3, the closed-form analytical solution for the transport of a band released single member decay chain via an arbitrary combination of fractured or porous transport segments is its use in benchmarking the TTBX code. As an example of the benchmarking performed, we present a case for the band release of three separate nuclides [94]Nb, ^{99}Tc, and [129]I along a heterogeneous pathway. These nuclides were chosen because their respective half-lives differ by at least an order of magnitude among them and cover the ranges of 2×10^4 years to 1.5×10^7 years. The pathway consists of three segments, two fractured segments followed by one porous segment, of lengths 100 m, 400 m, and 500 m respectively, for a total transport length of 1000 m. We do not consider the effects of sorption along the transport pathway, or with the host rock material in the fractured transport segments, although we do consider the effects of matrix diffusion via the parameter D_p which is varied along the transport pathway. The cross-sectional area of the transport pathway is considered remain fixed across all transport segments and is equal to 10^{-2} m². The remaining parameters for the transport calculation can be found in Tables 1 and 2.

Table 1
Assumed parameters for use in band release transport calculations.

Porosity of the fractured transport segments, ε_p	0.25
Water velocities in the fractures, v_1 and v_2 (m/yr) (first and second segments)	5.0 and 10.0
Fracture hydraulic aperture, $2b$ (m)	1.00E−02
Porosity of the porous transport segment, ε_a	0.3
Water velocity in the porous transport segment, v_3	15.0
Area of alluvial entrance (m^2)	1.00E−02
Length of Band Release, T(year)	3.00E+05
Characteristic width of fractures, w_p (m)	1
Length of fractured transport segments, L_1 and L_2 (m)	100 and 400
Length of porous transport segment, L_3 (m)	500

Table 3 shows the results of the comparison between the analytical solution developed in Section 3.3, and the results obtain via the numerical inversion of the LTAS using the TTBX computer code. As we can see in the region in which the numerical solutions converge we are able to achieve good agreement. In fact, the relative error in the calculations is seen to exceed 1% only in those times which are approximately fifty half-lives of the radionuclide

under consideration. Because there is no sorption along the transport pathway we can easily calculate that transport time of each of the nuclides to the 1 km observation point will be slightly more than 93 years, indeed we can see that the analytical solution produces a zero concentration result for times less than or equal to 100 years.

It is well known that given a step function $h(t - T)$ that Talbot's method produces unstable results for times $t < T$ (Murli and Rizzardi, 1990), therefore it is expected that TTBX will not give accurate results for times less than approximately 100 years in this case. However, we see that TTBX solutions are not accurate until 1000 years in this case so that we miss the initial arrival of the nuclides while their concentration is quite low. Further, we see that TTBX fails to be accurate in times which are greater than fifty half-lives of the radionuclide in question. However, this still represents a rather large span of time and captures the vast majority of the important aspects of the radionuclide concentration, including the initial rise of the concentration, the peak value of the concentration, and its ultimate decline. We can say from these results that TTBX compares favorably with the analytical solution within its region of convergence for a large span of time and that the results

Table 2
Inventory, diffusion coefficient, retardation and capacity factors in band release transport calculations.

Nuclide	Half-Life (years)	Inventory (At 1000 yr) (mol)	Fractured transport segments			All segments
			α_e (all)	D_e (m^2/yr) (1st segment)	D_e (m^2/yr) (2nd segment)	R_e
^{94}Nb	2.03E+04	1.00E+00	2.50E−01	1.00E−03	1.00E−02	1.00E+00
^{99}Tc	2.13E+05	1.00E+00	2.50E−01	1.00E−03	1.00E−02	1.00E+00
^{129}I	1.57E+07	1.00E+00	2.50E−01	1.00E−03	1.00E−02	1.00E+00

Table 3
Comparison of TTBX with band-release analytical solution.

Time (yr)	Concentration ^{129}I (mol/m^3)		Concentration ^{99}Tc (mol/m^3)		Concentration ^{94}Nb (mol/m^3)	
	TTBX	Relative error (%)	TTBX	Relative error (%)	TTBX	Relative error (%)
1.00E+00	–		–		–	
2.15E+00	–		–		–	
4.64E+00	–		–		–	
1.00E+01	–		–		–	
2.15E+01	–		–		–	
4.64E+01	–		–		–	
1.00E+02	–		–		–	
2.15E+02	x		x		x	
4.64E+02	x		x		x	
1.00E+03	1.19E−11	1.63E−04	1.18E−11	1.06E−04	1.15E−11	1.58E−04
2.15E+03	6.87E−08	3.15E−04	6.82E−08	2.39E−04	6.37E−08	1.99E−06
4.64E+03	3.37E−06	2.38E−05	3.32E−06	4.50E−05	2.87E−06	7.80E−08
1.00E+04	2.22E−05	3.93E−05	2.15E−05	6.29E−05	1.57E−05	1.28E−04
2.15E+04	5.85E−05	3.37E−04	5.46E−05	3.89E−04	2.77E−05	7.47E−05
4.64E+04	9.91E−05	3.33E−05	8.53E−05	1.53E−04	1.99E−05	1.05E−04
1.00E+05	1.34E−04	1.22E−04	9.68E−05	1.21E−04	4.20E−06	7.23E−06
2.15E+05	2.08E−05	7.93E−05	1.04E−05	4.66E−05	1.20E−08	3.20E−05
4.64E+05	5.22E−06	4.01E−04	1.17E−06	1.31E−04	5.49E−13	7.25E−05
1.00E+06	1.49E−06	1.21E−04	5.89E−08	1.84E−04	1.35E−21	2.07E+00
2.15E+06	4.33E−07	9.84E−06	4.13E−10	2.99E−05	x	
4.64E+06	1.22E−07	2.30E−05	3.78E−14	6.25E−06	x	
1.00E+07	3.07E−08	2.62E−05	3.02E−22	3.48E+00	x	
2.15E+07	6.05E−09	7.93E−05	x		–	
4.64E+07	6.93E−10	2.73E−04	x		–	
1.00E+08	2.46E−11	4.80E−05	x		–	
2.15E+08	7.03E−14	2.69E−04	–		–	
4.64E+08	8.77E−19	1.50E−02	–		–	
1.00E+09	x		–		–	
2.15E+09	x		–		–	
4.64E+09	x		–		–	
1.00E+10	x		–		–	

from TTBX capture the most important aspects of the evolution of the concentration at the observation point.

5. Application of TTBX code to a previously studied case

5.1. Cases considered

For this portion of the study, we have chosen the same case as previously reported in van den Akker and Ahn (2013), in which the annual dose received by the Reasonably Maximally Exposed Individual (RMEI) from the disposal of Deep-Burn Modular High Temperature Reactor (DBMHR) spent fuel (DBSF) was evaluated for the proposed Yucca Mountain Repository (YMR). In the previous study (van den Akker and Ahn, 2013), the TTB code was used, i.e., a 1-D homogeneous transport path, which connects the source (the waste package in the repository) and the evaluation point (18 km down gradient), while three distinct regions in the saturated zone in the far-field region were observed in the TSPA-LA study (Wu, 2003). By using the new TTBX model for the multiple-segment pathway with the same source conditions assumed in van den Akker and Ahn (2013), we can observe the effects of the assumption for the pathway heterogeneity. The source conditions assumed in van den Akker and Ahn (2013) are summarized for the reader's convenience in Table 4 for the radionuclide inventory in a waste package, and Table 5 for the parameters for transport in the spherical near-field region.

The drifts in the YMR are situated some 300 m below the ground surface and about 300 m above the water table. Once radionuclides have been released from the waste packages, they must traverse the unsaturated zone in order to reach the saturated zone where they can be transported down gradient through a network of fractures to the alluvium and subsequently to the RMEI, located a total distance of 18 km down gradient from the repository.

Table 4
DBSF radionuclide inventory.

Nuclide	Half-life (years)	DBSF (At Package Failure t = 0) (mol)
^{14}C	5.72E+03	9.35E−07
^{79}Se	2.95E+05	2.52E−02
^{90}Sr	2.88E+01	5.05E−11
^{99}Tc	2.13E+05	4.50E+00
^{126}Sn	2.50E+05	1.11E−01
^{129}I	1.57E+07	4.08E−02
^{135}Cs	2.30E+06	2.67E+00
^{137}Cs	3.01E+01	5.16E−10
^{210}Pb	2.23E+01	1.16E−06
^{226}Ra	1.60E+03	8.43E−05
^{228}Ra	5.76E+00	5.90E−15
^{227}Ac	2.18E+01	5.08E−11
^{229}Th	7.30E+03	3.53E−06
^{230}Th	7.54E+04	1.85E−02
^{232}Th	1.40E+10	1.44E−05
^{231}Pa	3.28E+04	7.88E−08
^{237}Np	2.14E+06	7.57E+00
^{232}U	6.98E+01	3.11E−10
^{233}U	1.59E+05	1.90E−03
^{234}U	2.46E+05	7.62E+00
^{235}U	7.04E+08	5.37E−02
^{236}U	2.34E+07	9.69E−01
^{238}U	4.47E+09	2.70E−02
^{238}Pu	8.77E+01	2.93E−03
^{239}Pu	2.41E+04	1.27E+00
^{240}Pu	6.56E+03	8.64E+00
^{241}Pu	1.40E+01	4.18E−04
^{242}Pu	3.75E+05	1.48E+01
^{241}Am	4.33E+02	1.15E+00
^{243}Am	7.37E+03	3.09E+00
^{245}Cm	9.30E+03	2.53E−01

Table 5
Parameters in the spherical near-field region.

Element	Solubility N_e * (mol/m^3) Sandia National Laboratories (2007) and van den Akker and Ahn (2011)	Diffusion coefficient in the fractured volcanic rock D_e^f (m^2/yr) Reimus (2004)	Retardation factor in the diffusion barrier R_e
Americium	8.88E+02	1.58E−03	2.67E+03
Plutonium	4.23E+02	1.58E−03	6.68E+02
Uranium	9.69E+01	1.58E−03	2.33E+00
Neptunium	1.65E+02	1.58E−03	7.66E+00
Thorium	2.61E+01	1.58E−03	3.67E+04
Protactinium	1.65E+02	1.58E−03	3.67E+04
Radium	3.09E+02	1.58E−03	2.17E+03
Technetium	–	1.58E−03	1.00E+00
Carbon	–	1.58E−03	1.00E+00
Strontium	–	1.58E−03	1.68E+02
Selenium	–	1.58E−03	5.83E+01
Tin	5.01E−05	1.58E−03	4.73E+03
Iodine	–	1.58E−03	1.00E+00
Cesium	–	1.58E−03	1.43E+01

Porosity of the diffusion barrier region, ε (Liu, 2007)	0.229
Density of the diffusion barrier region, ρ (kg/m^3) (Kuzio, 2004)	1980
Surface area of the diffusion barrier region (m^2)	50.82
Graphite waste-form oxidation rate, R (g/m^2/d),	1.70E−08
Mass of graphite being degraded (g)	8.77E+00
Distance between two waste forms (m) (Richards, 2002)	5.24

Transport of radionuclides in the saturated zone occurs, then, in two regions. In the first 13 km down-gradient from the repository, transport occurs via advection in the fractures of fractured volcanic rock. At the 13 km location, the radionuclides enter the alluvial zone, where transport takes place as advection through a porous medium for the next 5 km (Sandia National Laboratories, 2008). In the previous study (van den Akker and Ahn, 2013), however, the entire 18-km pathway was treated as a single homogeneous conduit by claiming that transport time is significantly shorter through the fracture network than in the alluvium (Sandia National Laboratories, 2008). In the present study, the transport of radionuclides in the first 13 km of the pathway in the saturated zone is divided into two segments: 5 km and 8 km. In these two segments, transport occurs via advection in the fractures of the fractured volcanic rock. These segments are considered as "fractured" media with matrix diffusion. The difference between the 5-km and 8-km segments is the value of the water velocity in the fracture in those segments, 0.87 m/yr and 7.50 m/yr, respectively. At the 13 km location, the radionuclides enter the alluvial zone, where transport takes place as advection through a porous medium for the next 5 km (Sandia National Laboratories, 2008). Thus, three distinct segments along the 18-km pathway are considered in the present calculation, whereas in the previous study the same pathway was treated as a single homogeneous region. Parameter values related to the far-field transport are summarized in Table 6. Note that data need to be specified for each segment.

The annual dose to the RMEI is calculated by evaluating Eq. (42) taken from Wu (2003) for exposure via contaminated groundwater:

$$D_T(x,t) = \sum_{j=1}^{N} BDFC_j \cdot C_j(x,t) \tag{42}$$

The biosphere dose conversion factor (BDCF) is a means of translating concentration of radionuclides in the groundwater at the observation location into an annual dose received by the RMEI for the

Table 6
Values for transport parameters for three segments in the far-field region.

Element	Diffusion coefficient in the fractured volcanic rock (Segment2 1 and 2) D_e^l (m²/yr) Reimus, 2004	Capacity factor in the fractured volcanic rock (Segments 1 and 2) α_e	Retardation factor in the fracture (Segments 1 and 2) R_e	Retardation factor in the porous alluvium (Segment 3) R_e
Americium	1.58E−03	7.30E+03	1.00E+00	4.11E+04
Plutonium	1.58E−03	1.33E+02	1.00E+00	7.49E+02
Uranium	1.58E−03	1.59E+01	1.00E+00	3.54E+01
Neptunium	1.58E−03	3.82E+00	1.00E+00	4.85E+01
Thorium	1.58E−03	7.30E+03	1.00E+00	4.11E+04
Protactinium	1.58E−03	7.30E+03	1.00E+00	4.11E+04
Radium	1.58E−03	7.30E+02	1.00E+00	4.11E+03
Technetium	1.58E−03	2.50E−01	1.00E+00	1.00E+00
Carbon	1.58E−03	2.50E−01	1.00E+00	1.00E+00
Strontium	1.58E−03	2.79E+02	1.00E+00	1.57E+03
Selenium	1.58E−03	1.86E+01	1.00E+00	1.06E+02
Tin	1.58E−03	2.52E+03	1.00E+00	3.74E+05
Iodine	1.58E−03	2.50E−01	1.00E+00	1.00E+00
Cesium	1.58E−03	9.66E+02	1.00E+00	5.44E+03
		Segment 1	Segment 2	Segment 3
Porosity of the fractured volcanic rock, ε_p Kuzio (2004)		0.25	0.25	–
Density of the fractured volcanic rock, ρ_p (kg/m³) Kuzio (2004)		1770	1770	–
Water velocity in the fracture (homogeneous pathway) v (m/yr) Kuzio (2004)		7.50		
Fracture hydraulic aperture, $2b$ (m)		1.45E−01	1.45E−01	–
Water velocity in the fractures, (m/yr) Reimus (2004)		0.87	7.50	16.75
Porosity of the alluvium, ε_a Reimus (2004)		–	–	0.19
Density of the alluvium, ρ_a (kg/m³) Reimus (2004)		–	–	1754
Area of alluvial entrance (m²)		–	–	0.43
Characteristic fracture width w_p (m) Richards (2002) and Ahn (1998)		20.6		

Table 7
Biosphere dose conversion factors (Sandia National Laboratories, 2008).

Nuclide	BDCF (Sv/yr per Bq/m³)	Nuclide	BDCF (Sv/yr per Bq/m³)	Nuclide	BDCF (Sv/yr per Bq/m³)
[14]C	1.93E−09	[227]Ac	1.30E−06	[238]U	7.87E−08
[79]Se	2.42E−08	[228]Th	3.15E−07	[237]Np	2.74E−07
[90]Sr	3.43E−08	[229]Th	2.58E−06	[238]Pu	7.61E−07
[99]Tc	1.12E−09	[230]Th	1.08E−06	[239]Pu	9.55E−07
[126]Sn	4.33E−07	[232]Th	1.85E−06	[240]Pu	9.51E−07
[129]I	1.29E−07	[231]Pa	2.44E−06	[242]Pu	9.07E−07
[135]Cs	1.45E−08	[232]U	6.04E−07	[241]Am	8.34E−07
[137]Cs	1.30E−07	[233]U	8.97E−08	[243]Am	8.88E−07
[210]Pb	2.74E−06	[234]U	8.19E−08		
[226]Ra	3.78E−06	[235]U	9.41E−08		
[228]Ra	9.05E−07	[236]U	7.67E−08		

exposure pathway through groundwater transport to the observation point. In the present study, we use the same value as used in van den Akker and Ahn (2013), which is the mean value of the BDCF for each radionuclide in the current climatic conditions (Sandia National Laboratories, 2008). These values are given in Table 7.

The previous study (van den Akker and Ahn, 2013) considered optimistic, nominal, and pessimistic environmental cases by varying the hydro-geological parameters associated with radionuclide transport. Only the pessimistic environmental case will be considered in the present study. Further details may be obtained in van den Akker and Ahn (2013).

5.2. Numerical results

Fig. 3 shows the results of radionuclide transport calculations considering a homogeneous transport pathway via a single 18 km fracture, the same as those published in van den Akker and Ahn (2013). In this case we observe that main contributors to the annual dose delivered to the RMEI are ^{99}Tc, [237]Np, and [227]Ac. Fig. 4 shows the results for the same source conditions as

those for Fig. 3 but considering the heterogeneous transport pathway described in Section 5.1. We see here that much like the homogeneous pathway results, the major contributors to the annual dose received by the RMEI are ^{99}Tc, [237]Np, and [227]Ac. However, in Fig. 5 comparing the total annual dose shown in Fig. 4 with that in Fig. 3, we see that the maximum annual dose received by the RMEI is more than two orders of magnitude lower when calculated using the heterogeneous pathway, relative to the homogeneous pathway. This difference can be attributed to the initial slow flow region in the first 5 km segment in the multi-region pathway, coupled with relatively strong sorption of two main contributors [237]Np, and [235]U. Although [235]U is not directly seen as a main contributor to the overall dose, its decay daughter [227]Ac (which is in secular equilibrium with [235]U because of the difference in the half-lives) is a main contributor in the longer time periods. This is largely because the long lifetime of the graphite matrix allows for the ingrowth of [227]Ac, and because of the relatively high value of the BDCF for [227]Ac. It is interesting to note that the TSPA results for the YMR typically show [129]I, [237]Np, and ^{99}Tc as the top dose contributors depending on the time after emplacement. However in this study, the top contributors were ^{99}Tc, [237]Np, and [227]Ac.
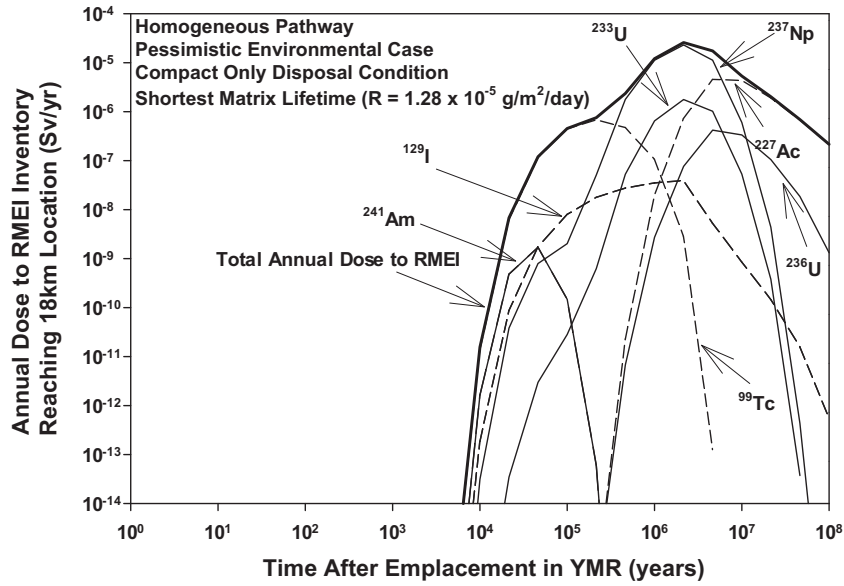
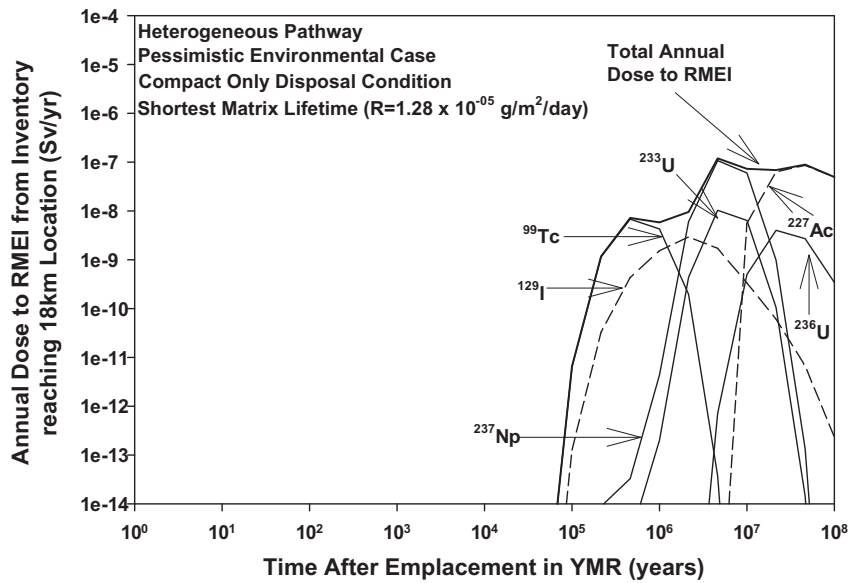**Fig. 3.** Annual dose to the RMEI in the pessimistic environmental case from flow along a homogeneous pathway.

Fig. 4. Annual dose to the RMEI in the pessimistic environmental case from flow along a heterogeneous pathway.

We see that ^{239}I is lower in the present study, because it is assumed that the whole inventory of iodine is contained in the graphite waste form, whereas in the YMR TSPA for commercial spent fuel disposal, a small fraction (3%) is assumed to be released very early due to the fact that it is in the gap between the fuel cladding and the pellet. So, a narrow and high peak of iodine is formed, which determines the max dose of iodine.

6. Discussion

The results of this analysis show that annual dose calculated to be received by the RMEI from the disposal of DBSF in the YMR was overestimated when smearing a heterogeneous transport pathway by a homogeneous transport pathway, and assigning properties of the entire 18-km region with the fast-flow region. This highlights the sensitivity of the hydrogeological parameters associated with

radionuclide transport models and of assumptions employed in the conceptual model, and thus the need for models sufficiently generic to accommodate these heterogeneities.

The simplification made in the previous study (van den Akker and Ahn, 2013) may be considered allowable because the results were regarded as conservative; the overestimated concentrations result in pessimistic estimates of the annual dose. But, we can confirm conservatism in assessment results only by accumulating such comparative studies as the present study among various models with different degrees of fidelity, because validation of models by direct comparison with experimental or in-situ measurements is not possible for the timeframe of a performance assessment. In this regard, the present study has added an important insight for results of performance assessment, which should serve to build confidence in the performance assessment process.
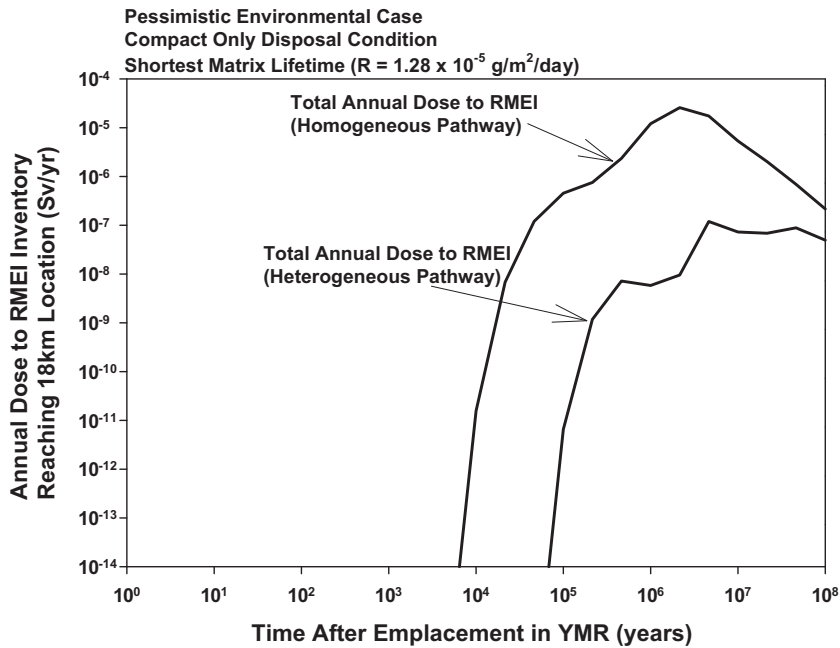
Fig. 5. Comparison of annual dose received by RMEI calculated by homogeneous and heterogeneous pathway calculations.

7. Conclusions

In this study we have presented two solutions to the problem of radionuclide transport through heterogeneous geological media. We have developed the Laplace-transformed analytical solutions (LTAS) for the transport of an arbitrary length decay chain via an arbitrary combination of fractured and porous media for a generic time-dependent source term whose Laplace transform may be written in terms of analytic functions and which converges suitably as the Laplace variable $|s| \rightarrow \infty$.

As a special case, and for the purposes of benchmarking the newly-developed TTBX code, we have also developed a closed-form analytical solution to the problem of the band release of a single member decay chain and subsequent transport via an arbitrary combination of fractured and porous media. This analytical solution provides a fast and convenient method for the quantification of radionuclides, particularly (but not limited to) important fission products such as ^{129}I and ^{99}Tc, released and transported in the environment.

The numerical inversion of the LTAS has been performed using Talbot's Method in the TTBX code. TTBX includes the same source term function based on a spherical near-field region containing a waste form and the diffusion barrier as does TTB. The benchmark results show good agreement with the analytical solution for the band release with a single nuclide for a wide range of time.

Using the TTBX code, numerical demonstration has been made for the same case as was reported in van den Akker and Ahn (2013) for the case of geological disposal of spent TRISO fuels from the Deep-Burn Modualar High Temperatue Reactor in the Yucca Mountain repository. In the present study, the transport pathway in the far field region was divided into three segments, as was described in the TSPA-LA study (Wu, 2003), while in van den Akker and Ahn (2013) the far-field pathway was homogenized into a single segment. The results indicate that untested homogenization applied in the previous study resulted in more than two-orders of magnitude overestimation of annual dose, because the previous study adopted the transport parameters of the fastest segment to the entire pathway. Thus, we could confirm conservatism of the previous

study. Also, the present model for multiple segments will help improve fidelity and reliability of the performance assessment.

References

Ahn, J., 1998. Integrated radionuclide transport model for a high-level waste repository in water-saturated geological formations. Nucl. Technol. 121 (1), 24–39.

Ahn, J., Suzuki, R., Kiyose, R., 1984. Numerical analysis of nuclide migration through fissured geological media. Nucl. Technol. 64, 154–164.

Arriaza, J.L., Ghezzehei, T.A., 2013. Explaining longitudinal hydrodynamic dispersion using variance of pore size distribution. J. Porous Media 16 (1), 11–19.

Chambré, P.L., Pigford, T.H., Fujita, A., Kanki, T., Kobyashi, A., Lung, H., Ting, D., Sato, Y., Zavoshy, S.J., 1982. Analytical Performance Modles for Geological Repositories, LBL-14842. Lawrence Berkeley National Laboratory, Berkeley, CA.

Grisak, G.E., Pickens, J., 1980. Solute transport through fractured media, I, the effect of matrix diffusion. Water Resour. Res. 16, 719.

Hodgkinson, D.P., Maul, P.R., 1988. 1-D modelling of radionuclide migration through permeable and fractured rock for arbitrary length decay Cahins using numerical inversion of Laplace transforms. Ann. Nucl. Energy 15 (4), 175–189.

Kuzio, S., 2004. Probability Distribution for Flowing Interval Spacing. Office Of Civilian Radioactive Waste Management, Las Vegas, Nevada, USA.

Liu, H., 2007. Calibrated Unsaturated Zone Properties. Office of Civilian Radioactive Waste Management, Las Vegas, Nevada, USA.

Murli, A., Rizzardi, M., 1990. Algorithm 682 Talbot's method for the Lapace inversion problem. ACM Trans. Math. Softw. 16 (2), 158–168.

Neretnieks, I., 1980. Diffusion in the rock matrix: an important factor in radionuclide retardation? J. Geophys. Res. 89 (B8), 4379–4397.

Rasmuson, A., Nereetnieks, I., 1981. Migration of radionuclides in fissured rock: the influence of micropore diffusion and longitudinal dispersion. J. Geophys. Res. 86, 3746.

Rasmuson, A.T., Narasimhan, T., Neretnieks, I., 1982. Chemical transport in a fractured roc: verification of a numerical model. Water Resour. Res. 18, 1479.

Reimus, P.W., 2004. Saturated Zone In-Situ Testing. Office of Civilian Radioactive Waste Management, Las Vegas, Nevada, USA.

Richards, M., 2002. Assessment of GT-MHR Spent Fuel Characteristics and Repository Performance. General Atomics, San Diego.

Sandia National Laboratories. 2008. Total System Performance Assessment Model/ Analysis for License Application. U.S. Department of Energy Office of Civilian Radioactive Waste Management, Las Vegas, NV.

Sandia National Laboratories. 2007. Dissolved Concentration Limits of Elements with Radioactive Isotopes. Sandia National Laboratories, Sandia, New Mexico, USA.

Singhal, B., Gupta, R.P, 2010. Principles of Groundwater Flow and Solute Transport. In: Applied Hydrogeology of Fractured Rocks. Springer, Netherlands, pp. 115–138.

Sudicky, E.A., Frind, E.O., 1984. Contaminant transport in fractured porous media: analytical solution for a two-member decay chain in a single fracture. Water Resour. Res. 20, 2021.

Talbot, A., 1978. The accurate numerical inversion of laplace transforms. J. Inst. Maths Appl. 23, 97–120.

Tang, D., Frind, E.O., Sudicky, E., 1981. Contaminant transport in fractured porous media: analytical solution for a single fracture. Water Resour. Res. 17, 555.

van den Akker, BP., 2012. On the Disposition of Graphite Containing TRISO Particles and the Aqueous Transport of Radionuclides via Heterogeneous Geological Formations. University of California at Berkeley, Ph.D Dissertation, Berkeley.

van den Akker, B.P, Ahn, J., 2011. Solubilities of radionuclides released from graphite waste calculated using PHREEQC. In: International High Level Radioactive Waste Management Conference. ANS, Albuquerque, New Mexico, USA.

van den Akker, B.P., Ahn, J., 2013. Performance assessment for geological disposal of graphite waste containing TRISO particles. Nucl. Technol. 181, 408–426.

Wu, D.W., 2003. Biosphere Model Report. United States Department of Energy, Las Vegas, Nevada, USA.